

RESEARCH ARTICLE

Open Access



The Role of Layer-Specific Residual Stresses in Arterial Mechanics: Analysis via a Novel Modelling Framework

Alessandro Giudici^{1,3,4*} and Bart Spronck^{2,3}

Abstract

The existence of residual stresses in unloaded arteries has long been known. However, their effect is often neglected in experimental studies. Using a recently developed modelling framework, we aimed to investigate the role of residual stresses in the mechanical behaviour of the tri-layered wall of the pig thoracic aorta. The mechanical behaviour of the intact wall and isolated layers of $n = 3$ pig thoracic aortas was investigated via uniaxial tensile testing. After modelling the layer-specific mechanical data using a hyperelastic strain energy function, the layer-specific deformations in the unloaded vessel were estimated so that the mechanical response of the computationally assembled tri-layered flat wall would match that measured experimentally. Physiological tension–inflation of the cylindrical tri-layered vessel was then simulated, analysing changes in the distribution of stresses in the three layers when neglecting residual stresses. In the tri-layered model with residual stresses, layers exhibited comparable stresses throughout the physiological range of pressure. At 100 mmHg, intimal, medial, and adventitial circumferential load bearings were $16 \pm 3\%$, $59 \pm 4\%$, and $25 \pm 2\%$, respectively. Adventitial stiffening at high pressures produced a shift in load bearing from the media to the adventitia. When neglecting residual stresses, *in vivo* stresses were highest at the intima and lowest at the adventitia. Consequently, the intimal and adventitial load bearings, $23 \pm 2\%$ and $18 \pm 3\%$ at 100 mmHg, were comparable at all pressures. Residual stresses play a crucial role in arterial mechanics guaranteeing a uniform distribution of stresses through the wall thickness. Neglecting these leads to incorrect interpretation of the layers' role in arterial mechanics.

Keywords: Residual stresses, Tri-layered arterial wall modelling, Intima, Media, Adventitia

1 Introduction

The arterial wall is characterised by a strong relationship between structure and function [1, 2], so that arterial structure varies considerably at different locations in the arterial tree [2]. Large elastic arteries are located in proximity of the heart. At a macroscopic level, these arteries are organised in three concentric layers, the intima, the media and the adventitia, each playing a pivotal role in

arterial function. The intima, the innermost layer, interacts directly with the blood flow and provides a small contribution to the wall's mechanics due to its small thickness. The media, the middle and thickest layer, determines the elastic behaviour that characterises large arteries at physiological pressures [3] and endows them with their blood pressure buffering (or Windkessel) function, which smooths the intermittent pumping action of the heart into a more continuous blood pressure ensuring organ perfusion also in diastole. The adventitia is the outermost layer and is typically described as a protective sleeve that preserves the wall's integrity at high pressures [2].

*Correspondence: a.giudici@maastrichtuniversity.nl

³ Department of Biomedical Engineering, CARIM School for Cardiovascular Diseases, Maastricht University, Universiteitssingel 50, Room 3.353, 6229 ER Maastricht, The Netherlands
Full list of author information is available at the end of the article



© The Author(s) 2022. **Open Access** This article is licensed under a Creative Commons Attribution 4.0 International License, which permits use, sharing, adaptation, distribution and reproduction in any medium or format, as long as you give appropriate credit to the original author(s) and the source, provide a link to the Creative Commons licence, and indicate if changes were made. The images or other third party material in this article are included in the article's Creative Commons licence, unless indicated otherwise in a credit line to the material. If material is not included in the article's Creative Commons licence and your intended use is not permitted by statutory regulation or exceeds the permitted use, you will need to obtain permission directly from the copyright holder. To view a copy of this licence, visit <http://creativecommons.org/licenses/by/4.0/>.

To fulfil their specific function, arterial layers differ significantly at the microstructural level. The intima is constituted mainly by endothelial cells, a thin basement membrane, a proteoglycan rich matrix and collagen fibres oriented in the axial direction [4, 5]. The media is organised in concentric medial lamellar units, alternating elastin-rich lamellae and inter-lamellar spaces composed of vascular smooth muscle cells, elastin and collagen fibres which are predominantly oriented in the circumferential direction [3, 4, 6]. The adventitia is mainly constituted by bundles of diagonally oriented collagen fibres, showing larger angular dispersion than in the media. Further, unlike the intima and the media, the adventitia is relatively acellular [7, 8].

Understanding the role each layer plays in arterial function has been the objective of several investigations, using different experimental techniques such as selective enzymatic digestion of specific wall constituents [9, 10] and imaging the wall's microstructure at different levels of distending pressure [3, 11, 12]. The separation and mechanical testing of isolated layers is a useful technique that directly assesses how their different microstructures determine their mechanical behaviour. This technique has been used to characterise the layer-specific mechanics in several arterial locations, species and in both physiological and pathological conditions [13–19]. Moreover, constitutive modelling, i.e. fitting structurally motivated mathematical models that describe the wall's mechanical behaviour as the summed contribution of the response of its constituents, has allowed investigating how layer-specific microstructural features affect the layer's mechanical properties, including anisotropy and recruitment of collagen fibres [13–19].

While characterising the behaviour of isolated layers provides some insight into the tri-layered arterial wall mechanics, it is not sufficient to fully understand their role in the macroscopic behaviour of arteries. Indeed, while an excised unloaded artery is subjected to null external loads in all three principal directions (i.e. circumferential, radial and axial), local stresses at any generic point within the arterial wall's volume are, in general, non-zero [20, 21]. As shown in previous studies [22–24], this particular feature of arteries likely arises from the fact that their wall develops and remodels in its loaded state (i.e. in vivo), attempting to preserve a uniform distribution of stresses throughout its thickness. When all external loads are removed, however, its inhomogeneous material properties and in vivo deformation field lead to the existence of residual stresses.

Residual stresses were first discovered in 1983 when two studies [21, 25] observed that, when cut radially, an arterial ring typically does not retain its circular shape but springs open and assumes an arc shape. This implies that

the unloaded vessel represents an equilibrium configuration between residual stresses acting throughout the arterial wall thickness that are compressive and tensile in the inner and outer part of the wall, respectively [26]. When a radial cut is performed, the geometrical constraint that guarantees this equilibrium is lost and the artery deforms to release said residual stresses, reaching a new equilibrium in its stress-free configuration. Knowledge of the inverse of this deformation is, therefore, crucial to determine the layer-specific prestress in the artery unloaded state and constitutes the link to fully understand the complex tri-layered mechanics of the arterial wall.

The circumferential component of this deformation is commonly quantified via an opening angle (OA), e.g. the angle formed by connecting the two endpoints of the arc-shaped circumferential wall sample to its mid-point [22]. Knowledge of the OA allows estimating the distribution of the circumferential deformation throughout the wall thickness of the unloaded artery, thus allowing to determine its pre-stressed state [23]. Further, a more comprehensive characterisation of the layer-specific three-dimensional geometry of excised circumferential and axial wall strips allows formulating complex models that predict the distribution of residual stresses in all three principal directions throughout the wall thickness [20, 27]. However, the implementation of such models is non-trivial and residual stresses are often neglected when modelling the tri-layered arterial wall [28, 29].

We recently developed a new tri-layered modelling framework that allows accounting for layer-specific residual stresses using only intact wall and layer-specific uniaxial test data [30]. Using the newly developed modelling framework, the present study aimed to illustrate the effects of residual stresses on arterial mechanics and how neglecting these can lead to considerable misinterpretation of the specific role arterial layers play in the macroscopic behaviour of the arterial wall. We will simulate three different scenarios: (1) a complete model with residual stresses, (2) a model where the unloaded vessel is considered stress free (i.e. completely neglecting all residual stresses), and (3) a model where a flat slab of wall tissue (as typically tested in planar biaxial tensile experiment) is used as an approximation of a cylindrical vessel.

2 Methods

2.1 Theoretical Background

2.1.1 Tri-layered Wall Model

A complete description of the mathematical formulation of the tri-layered wall model can be found in our previous study [30]. Briefly, the arterial wall is assumed to be comprised of three adequately spaced membranes representing the intima, media, and adventitia. The composition of the wall from isolated layers to unloaded cylindrical vessel is

described via two mapping steps: first, the three layers are assembled into a flat rectangular slab of arterial wall tissue. Due to the presence of residual stresses, layers change their shape when isolated from the wall. The layer-specific deformation gradient \mathbf{G}^k (where $k \in \{i, m, a\}$, i =intima, m =media, and a =adventitia) describes the inverse of this process, i.e. the deformation from the isolated layer configuration κ_{isolated} in Cartesian coordinates $(\mathcal{X}, \mathcal{Y}, \mathcal{Z})$ to tri-layered flat wall slab $\kappa_{\text{composite}}$ in $(\mathbb{X}, \mathbb{Y}, \mathbb{Z})$. For each layer k ,

$$\mathbf{G}^k = \text{diag} \left[\widehat{\lambda}_{\mathbb{X}}^k, \frac{1}{\widehat{\lambda}_{\mathbb{X}}^k \widehat{\lambda}_{\mathbb{Z}}^k}, \widehat{\lambda}_{\mathbb{Z}}^k \right], \tag{1}$$

where $\widehat{\lambda}_{\mathbb{X}}^k = l_{\mathbb{X}}/L_{\mathcal{X}}^k$ and $\widehat{\lambda}_{\mathbb{Z}}^k = l_{\mathbb{Z}}/L_{\mathcal{Z}}^k$ are the circumferential and axial components of \mathbf{G}^k , $l_{\mathbb{X}}$ and $l_{\mathbb{Z}}$ are the circumferential and axial dimensions of the composite wall, and $L_{\mathcal{X}}^k$ and $L_{\mathcal{Z}}^k$ are the circumferential and axial lengths of the isolated layer k . Note that the radial stretch is determined from incompressibility [31].

The second mapping step describes the deformation of the flat tri-layered wall, $\kappa_{\text{composite}}$, into an unloaded cylindrical vessel, κ_{unloaded} in cylindrical coordinates (Θ, R, Z) . The related deformation gradient is

$$\mathbf{F}_1 = \text{diag} \left[\Lambda_{\Theta}, \frac{1}{\Lambda_{\Theta} \Lambda_Z}, \Lambda_Z \right], \tag{2}$$

where the axial stretch Λ_Z is assumed to be constant throughout the wall and the circumferential component is calculated as

$$\Lambda_{\Theta} = \sqrt{\frac{4\pi^2 R_{\text{internal}}^2}{l_{\mathbb{X}}^2} + \frac{4\pi \mathbb{Y}}{l_{\mathbb{X}} \Lambda_Z}}, \tag{3}$$

where R_{internal} is the radius of the artery at the luminal surface.

The layer-specific residual stresses in κ_{unloaded} arise from the total deformation from κ_{isolated} to κ_{unloaded}

$$\mathbf{F}_{\text{residual},k} = \mathbf{F}_1 \mathbf{G}^k = \text{diag} \left[\Lambda_{\Theta} \widehat{\lambda}_{\mathbb{X}}^k, \frac{1}{\Lambda_{\Theta} \widehat{\lambda}_{\mathbb{X}}^k \Lambda_Z \widehat{\lambda}_{\mathbb{Z}}^k}, \Lambda_Z \widehat{\lambda}_{\mathbb{Z}}^k \right]. \tag{4}$$

The deformation gradient \mathbf{F}_2 maps the tension–inflation of the cylindrical vessel to a simulated in vivo configuration, $\kappa_{\text{tension–inflation}}$ in cylindrical coordinates (θ, r, z) . As for \mathbf{F}_1 , the axial component of \mathbf{F}_2 (λ_z) is assumed to be constant throughout the wall. \mathbf{F}_2 is defined as

$$\mathbf{F}_2 = \text{diag} \left[\lambda_{\theta}, \frac{1}{\lambda_{\theta} \lambda_z}, \lambda_z \right], \tag{5}$$

with

$$\lambda_{\theta} = \sqrt{\frac{r_{\text{internal}}^2}{R^2} + \frac{R^2 - R_{\text{internal}}^2}{R^2 \lambda_z}}, \tag{6}$$

where r_{internal} is the luminal radius in $\kappa_{\text{tension–inflation}}$.

The total deformation each layer is subjected to in $\kappa_{\text{tension–inflation}}$ is given by

$$\begin{aligned} \mathbf{F}_{\text{total},k} &= \mathbf{F}_2 \mathbf{F}_{\text{residual},k} \\ &= \text{diag} \left[\lambda_{\theta} \Lambda_{\Theta} \widehat{\lambda}_{\mathbb{X}}^k, \frac{1}{\lambda_{\theta} \Lambda_{\Theta} \widehat{\lambda}_{\mathbb{X}}^k \lambda_z \Lambda_Z \widehat{\lambda}_{\mathbb{Z}}^k}, \lambda_z \Lambda_Z \widehat{\lambda}_{\mathbb{Z}}^k \right]. \end{aligned} \tag{7}$$

2.1.2 Layer-Specific Constitutive Modelling

The mechanical behaviour of the three isolated arterial layers was modelled using the Holzapfel–Gasser–Ogden (HGO) two fibre family strain energy function (SEF) [32]. The passive behaviour of each layer is assumed to be determined by the summed contribution of an isotropic matrix, typically associated with elastin, and two symmetrically oriented families of collagen fibres that determine the wall’s anisotropy:

$$\Psi^k = \mu^k (I_1 - 3) + \sum_{i=1}^2 \frac{c_1^k}{2c_2^k} \left(e^{c_2^k [\rho^k (I_1) + (1-3\rho^k) I_{4,i} - 1]^2} - 1 \right), \tag{8}$$

where μ^k is an isotropic stiffness-like parameter ($k \in \{i, m, a\}$, i =intima, m =media, and a =adventitia), c_1^k is a collagen stiffness-like parameter, c_2^k is a dimensionless collagen non-linearity parameter, and $\rho^k \in [0, \frac{1}{3}]$ is a fibre dispersion coefficient, with $\rho = 0$ denoting fully aligned and $\rho = \frac{1}{3}$ denoting fully dispersed fibres (i.e. isotropic behaviour). I_1 and $I_{4,i}$ are the first and fourth invariant of the right Cauchy–Green tensor, respectively, with $i \in \{1, 2\}$ indicating the collagen fibre family with principal orientation $\alpha_{1,2}^k = \{-\alpha^k, \alpha^k\}$ with respect to the circumferential orientation. Note that the layer-specific fibre orientation $\alpha_{1,2}^k$ was not derived from microscopy data but phenomenologically estimated from the measured mechanical behaviour. For this reason, these angles should not be regarded as exact measures of the fibre orientation in the arterial layers but rather as a general quantification of the collagen-induced tissue anisotropic properties.

The Cauchy stress tensor is defined as

$$\boldsymbol{\sigma}^k = -p \mathbf{I} + 2 \mathbf{F}_{\text{total},k} \frac{\partial \Psi^k}{\partial \mathbf{C}_{\text{total},k}} \mathbf{F}_{\text{total},k}^T, \tag{9}$$

where \mathbf{I} is the spatial second order identity tensor and p is the Lagrange multiplier enforcing incompressibility [31].

2.2 Experimental Methods

Three pig plucks (i.e. the content of the thorax: heart, thoracic aorta, lungs, trachea, and liver) (age 6–12 months) were purchased from a local abattoir (samples from school, UK). Delivered frozen, each pluck was immediately stored at -20°C in a laboratory

freezer until the day of testing when it was left to thaw at room temperature for ~4 h. The aorta was then carefully dissected from the rest of the tissues using a scalpel. Two circumferentially and two axially oriented arterial strips (approximately $4 \times 25 \text{ mm}^2$) were isolated from the region of the descending thoracic aorta characterised by the branching of the intercostal arteries. Their width and thickness were carefully measured three times along the strip length using a high precision digital caliper. The mean of the three measurements was used for later analysis. Each strip was then subjected to uniaxial tensile testing in its long direction using a high-resolution uniaxial tensile device (MFS Stage with 20N load cell, Linkam Scientific Ltd., UK) equipped with serrated jaws to prevent slipping of the sample. The inter-jaw distance was initially set to 15 mm and then slowly increased until the sample laid flat. This flat length was considered as the unloaded sample length. Strips were uniaxially tested up to a Cauchy stress of 250 kPa after performing five loading/unloading cycles up to the same Cauchy stress. After testing, each strip was separated into its three layers using tweezers, first carefully peeling the adventitia from the intima-media and then isolating the intima from the media. As done for the intact wall, the layer's dimensions were measured at three locations along the strip length and the average values used for later analysis. Then, each layer was tested following the same protocol described for the wall strips.

The wall's and layer's experimental Cauchy stress was calculated as [33]

$$\sigma_{ii,\text{exp}}^k = \frac{F}{A_0} \bar{\lambda}_i^k, \quad (10)$$

where F is the force measured by the load cell, A_0 is the sample unloaded cross-sectional area, and $\bar{\lambda}_i^k$ is the stretch in which direction i (circumferential or axial) the sample $k \in \{\text{wall}, i, m, a\}$ is loaded during the uniaxial test.

2.3 Parameter Estimation

The fitting routine of all the model parameters has been described previously [30], and is briefly summarised below.

2.3.1 Layer-Specific Constitutive Parameters

The five layer-specific constitutive parameters in Eq. 8 were fitted on the layer-specific mechanical data, minimising the error between the individual layer's experimental (Eq. 10) and modelled (Eq. 9) Cauchy stress in the loading direction for the uniaxial tests in the circumferential and axial direction simultaneously. Since the off-axis deformation $\bar{\lambda}_j^k$ (i.e. $j \in \{\text{axial}, \text{circumferential}\}$ corresponding to the loading directions $i \in \{\text{circumferential}, \text{axial}\}$) was not measured during the experiments, this was determined by imposing $\sigma_{jj}^k = 0$ and enforcing incompressibility.

2.3.2 Determination of the Layer-Specific Deformation

in κ_{unloaded}

As shown in Eq. 4, determining the layer-specific deformation gradient in κ_{unloaded} requires estimating \mathbf{G}^k and \mathbf{F}_1 . The axial and circumferential components of \mathbf{G}^k of the three layers were fitted on the mechanical data of the intact wall, simultaneously minimising the error between the wall experimental Cauchy stress (Eq. 10) and that obtained when simulating the uniaxial tensile test of the tri-layered composite wall in both circumferential and axial directions. The average modelled Cauchy stress of the composite wall was calculated as

$$\sigma^{\text{wall}} = \frac{h^i \sigma^i + h^m \sigma^m + h^a \sigma^a}{h^{\text{wall}}}. \quad (11)$$

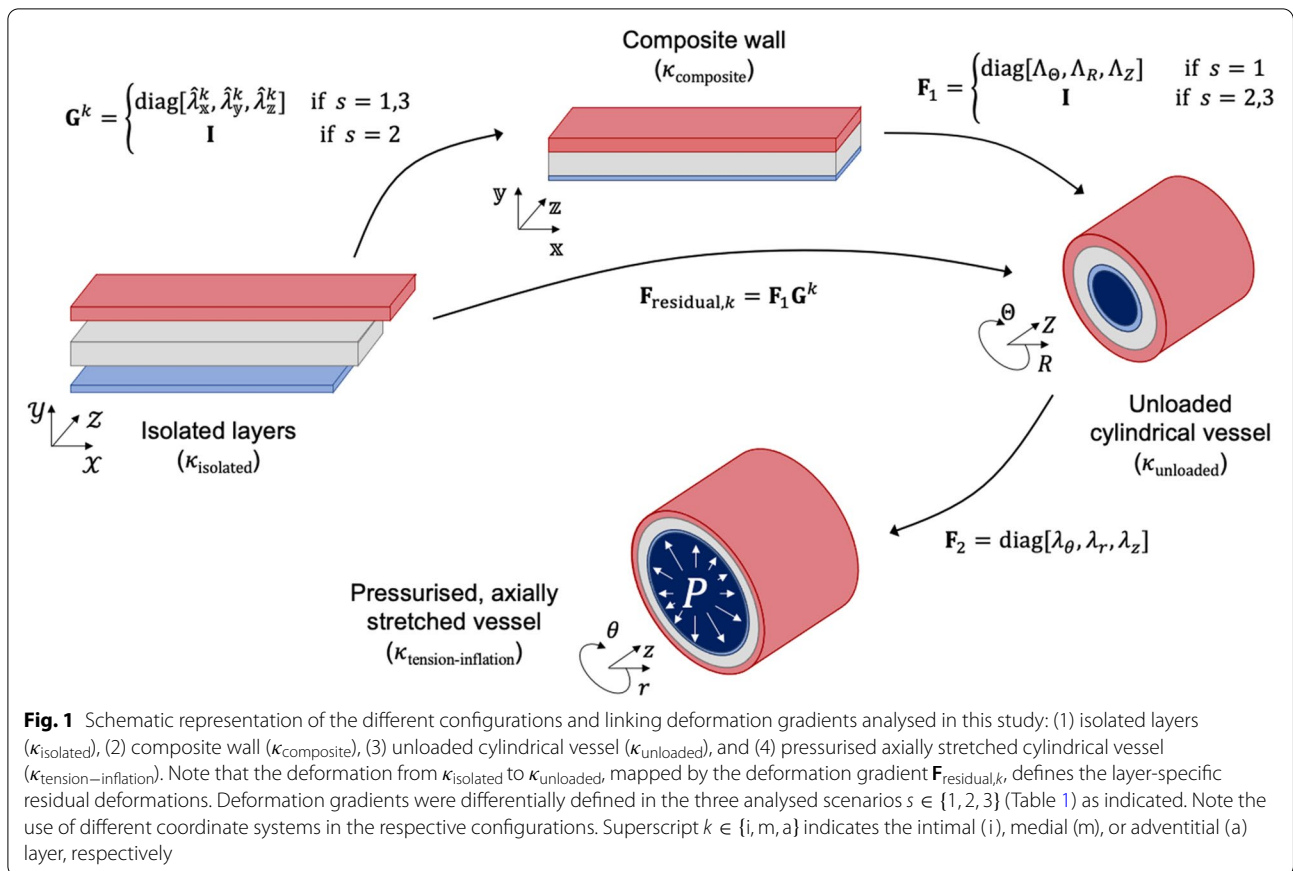
As described in the introduction, the unloaded configuration of the vessel (κ_{unloaded}) implies zero average wall stresses in all three principal directions. Therefore, Λ_Z and the layer-specific Λ_Θ were estimated iteratively by simultaneously minimising $\sigma_{\Theta\Theta}^{\text{wall}}$, $\sigma_{RR}^{\text{wall}}$, and $\sigma_{ZZ}^{\text{wall}}$.

2.3.3 Simulation of the Tension–Inflation

To assess the contribution of residual stresses to the wall mechanics, we simulated three tension–inflation scenarios: (1) full tri-layered model including layer-specific residual stresses ($\mathbf{F}_{\text{residual},k} = \mathbf{F}_1 \mathbf{G}^k$), (2) tri-layered model where residual stresses are completely neglected ($\mathbf{F}_{\text{residual},k} = \mathbf{I}$), and (3) assuming $\mathbf{F}_1 = \mathbf{I}$ ($\mathbf{F}_{\text{residual},k} = \mathbf{G}^k$) (Table 1 and Fig. 1). Case 1 represents the closest approximation of the in vivo condition; cases 2 and 3

Table 1 Description of the three modelling scenarios analysed in this study

Scenario	$\mathbf{F}_{\text{residual},k}$	Description
1	$\mathbf{F}_1 \mathbf{G}^k$	Layer-specific residual stresses in the unloaded cylindrical vessel (κ_{unloaded}) arise from two subsequent deformations of the isolated layers (κ_{isolated}): (1) into a tri-layered flat wall ($\kappa_{\text{composite}}$) that is (2) then bent into κ_{unloaded}
2	\mathbf{I}	Residual stresses in κ_{unloaded} are completely neglected as no deformation occurs from κ_{isolated} to κ_{unloaded}
3	\mathbf{G}^k	Layer-specific residual stresses in κ_{unloaded} arise solely from the deformation of the isolated layers (κ_{isolated}) into $\kappa_{\text{composite}}$. Hence, $\kappa_{\text{composite}}$ is used as an approximation of κ_{unloaded}



replicate two possible modelling approximations. In case 2, κ_{unloaded} is assumed to be a stress-free configuration (i.e. all three layers are undeformed in these configurations). In case 3, the flat arterial wall (which is the typical configuration of uniaxial and biaxial tensile tests) is assumed to be a good approximation of the cylindrical vessel, thus neglecting the deformation from $\kappa_{\text{composite}}$ to κ_{unloaded} .

Except for the definition of $\mathbf{F}_{\text{residual},k}$, all three cases followed the same modelling process. First, the simulated in vivo axial stretch λ_z was determined as the average cross-over point between simulated reduced axial force-axial stretch relationships at the distending pressure levels $P = 60, 100, \text{ and } 140 \text{ mmHg}$ [34]. The reduced axial force F_z was calculated as

$$F_z = \sum_{k=i,m,a} (2\pi \sigma_{zz}^k r^k h^k) - \pi r_{\text{internal}}^2 P, \quad (12)$$

where r^k is the mid-wall radius of the layer k . Given P , the corresponding r_{internal} was estimated iteratively to satisfy the Laplace equation

$$P = \sum_{k=i,m,a} (\sigma_{\theta\theta}^k - \sigma_{rr}^k) \frac{h^k}{r^k}. \quad (13)$$

Then, pseudo-physiological tension-inflation was simulated by axially stretching the vessel to λ_z and increasing luminal pressure from 0 to 200 mmHg.

Layer-specific and whole-wall stresses were determined using Eqs. 9 and 11, respectively. The percentage of load bearing for each layer was determined as

$$\text{Load bearing \%} = \frac{\sigma_{\theta\theta}^k h^k}{\sigma_{\theta\theta}^{\text{wall}} h^{\text{wall}}} \cdot 100\%. \quad (14)$$

The circumferential material stiffness $C_{\theta\theta\theta\theta}$ was calculated according to the small-on-large formulation [35] and evaluated continuously as a function of the distending pressure:

$$C_{\theta\theta\theta\theta} = 2(\sigma_{\theta\theta} + p) + 4\lambda_\theta^4 \frac{\partial^2 \Psi}{\partial (\lambda_\theta^2)^2}. \quad (15)$$

2.4 Statistical Analysis

For each aorta, tensile tests were conducted on two axially oriented and two circumferentially oriented strips. The layer-specific constitutive and tri-layered modelling was then conducted in pairs (i.e. circumferential strip 1 with axial strip

1 and circumferential strip 2 with axial strip 2) and the presented results of each artery are the mean of the two.

Results are presented as mean \pm standard deviation of the three tested aortas. Outcome parameters (wall stresses, material stiffness, load bearing %) were first evaluated continuously as a function of pressure. Then, comparison between modelling conditions (i.e. with and without residual stresses) was carried out at the reference normotensive mean arterial pressure (100 mmHg) and at 160 mmHg, representing the average hypertensive systolic pressure, using paired student's *t* tests. $p < 0.05$ was taken as statistically significant.

3 Results

3.1 Wall and Layer-Specific Response to Uniaxial Testing

The wall and layer geometrical features of the three pig thoracic aortas tested in this study are reported in Table 2. The mean radius and wall thickness were 7.79 ± 0.45 mm and 1.74 ± 0.31 mm, respectively. The isolated layer thicknesses were 0.28 ± 0.10 mm for the intima, 0.89 ± 0.24 mm for the media and 0.51 ± 0.07 mm for the adventitia, corresponding to $17 \pm 2\%$, $52 \pm 3\%$ and $31 \pm 1\%$ of the wall thickness, respectively.

Figure 2 presents the wall and layer-specific response to uniaxial tensile testing in both circumferential and axial directions. The wall was stiffer circumferentially than axially at stretches below 1.3 but became increasingly isotropic at higher deformations. This complex behaviour reflects the heterogeneity of the layer responses. Layer-specific model parameters of the three aortas are reported in Table 3. Both intima and media showed considerable anisotropy (Fig. 2), with α^k ranging from 36.2° – 38.9° (intima) and 28.8° – 35.5° (media), with respect to the circumferential direction. Conversely, the adventitia displayed a nearly isotropic behaviour (Fig. 2), if not slightly stiffer in the axial direction ($\alpha^a=43.0^\circ$ – 49.5°). Further, the non-linearity parameter c_2^k was more than an order of magnitude higher in the adventitia than in both intima and media, signifying a more pronounced stiffening (non-linearity) with increasing stretch.

3.2 Tri-layered Wall Modelling

3.2.1 Layer-Specific Deformation in κ_{unloaded}

The layer-specific components of the deformation gradients \mathbf{G}^k , \mathbf{F}_1 , and $\mathbf{F}_{\text{residual},k} = \mathbf{F}_1 \mathbf{G}^k$ are presented in Table 4. In the flat wall configuration $\kappa_{\text{composite}}$, the intima was subjected to tensile stretches in both circumferential and axial directions. Conversely, from κ_{isolated} to $\kappa_{\text{composite}}$, both media and adventitia experienced deformations of opposite nature in the circumferential and axial directions: circumferential extension and axial compression for the media and circumferential compression and slight axial extension for the adventitia. As expected, the deformation from $\kappa_{\text{composite}}$ to κ_{unloaded} (\mathbf{F}_1) introduced compressive and tensile circumferential deformations in the inner half and outer half of the wall thickness, respectively, with negligible deformations in the axial direction. As a result, the total circumferential deformation from κ_{isolated} to κ_{unloaded} ($\mathbf{F}_{\text{residual}}$) was strongly compressive (0.93 ± 0.01) for the intima, slightly tensile (1.01 ± 0.01) for the media, and tensile (1.04 ± 0.00) for the adventitia.

3.2.2 Simulated Tension–Inflation

Figure 3A–C presents the mean simulated pressure–diameter relationships for the three scenarios considered in this study (Table 1 and Fig. 1). Interestingly, while pressure–diameter relationships appeared very similar in the three considered scenarios, the distribution of stresses between the three layers differed considerably: First, in the full tri-layered wall model with residual stresses, $\sigma_{\theta\theta}$ – P and σ_{zz} – P relationships of the three layers appeared almost superimposed in the physiological pressure range (Fig. 4A, D). At a physiological pressure of 100 mmHg, $\sigma_{\theta\theta}$ and σ_{zz} were 0.078 ± 0.017 and 0.058 ± 0.014 MPa, 0.107 ± 0.013 and 0.062 ± 0.010 MPa, and 0.078 ± 0.012 and 0.067 ± 0.004 MPa for intima, media, and adventitia, respectively. The percentage of circumferential load borne by the media ($62 \pm 3\%$) was more than twice that of the adventitia ($24 \pm 2\%$) and four times that of the intima ($14 \pm 3\%$; Fig. 5A, B). When pressure increased to 160 mmHg, the corresponding increase in $\sigma_{\theta\theta}$ and σ_{zz} was comparable in the intima, $72 \pm 15\%$ and $38 \pm 11\%$, and media, $65 \pm 12\%$ and $34 \pm 7\%$, but

Table 2 Wall and layer geometrical features of the three pig thoracic aortas tested in this study

Sample #	<i>R</i> (mm)	<i>h</i> ^{wall} (mm)	<i>h</i> ^{intima} (mm)	<i>h</i> ^{media} (mm)	<i>h</i> ^{adventitia} (mm)
I	8.00	2.09	0.29	1.15	0.59
II	8.20	1.62	0.29	0.83	0.49
III	7.16	1.50	0.27	0.68	0.46
Mean \pm SD	7.79 ± 0.45	1.74 ± 0.25	0.28 ± 0.01	0.89 ± 0.19	0.51 ± 0.06

SD standard deviation

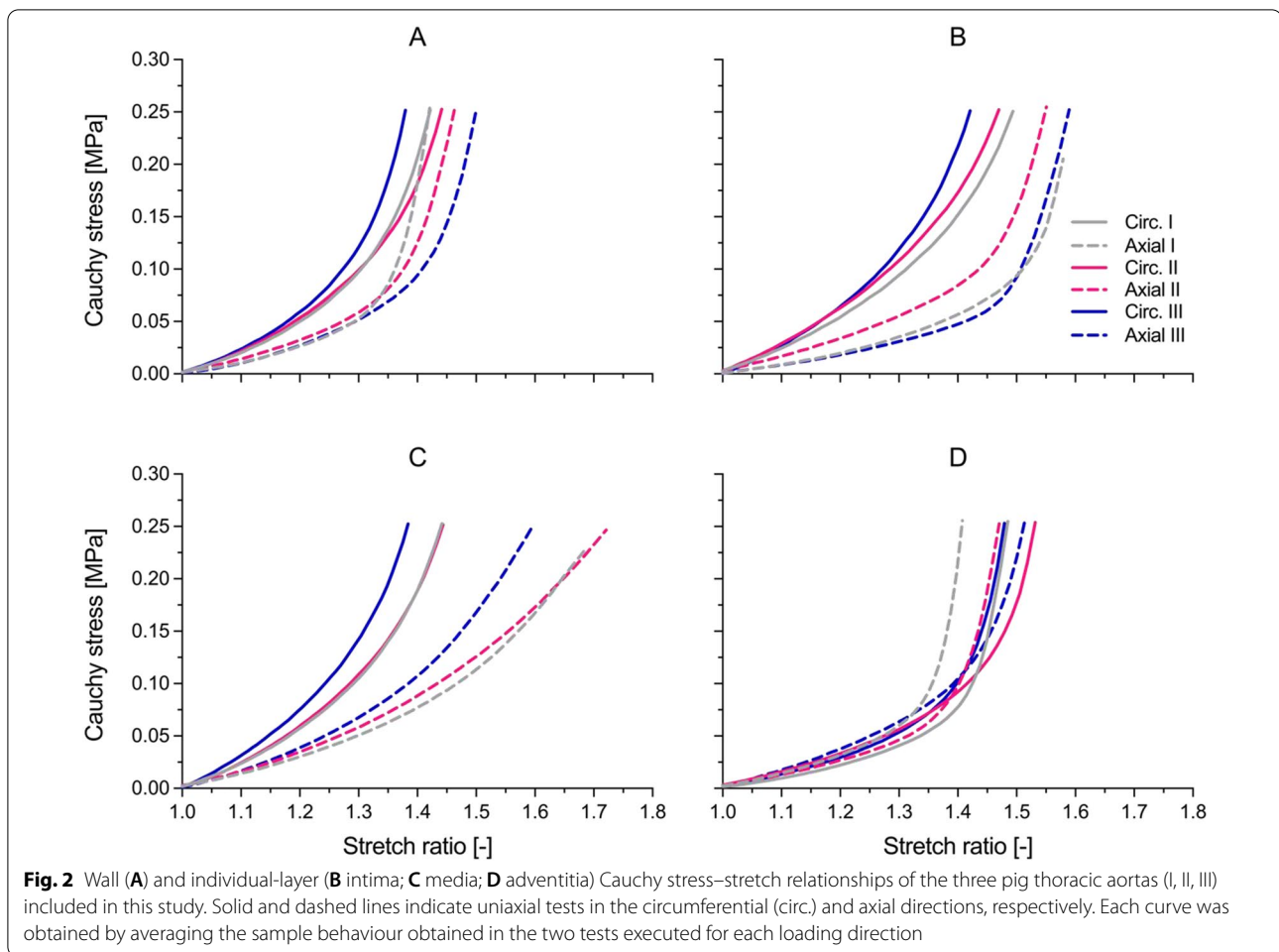


Table 3 Layer-specific parameters of the Holzapfel-Gasser-Ogden strain energy function of the three aortas included in this study

Layer	Sample #	μ^k (kPa)	c_1^k (kPa)	c_2^k (-)	α^k (°)	ρ^k (-)	R^2
Intima	I	12.7	163.5	0.1	36.6	0.20	0.98
	II	22.7	165.8	3.3	38.9	0.21	0.97
	III	6.5	249.5	1.1	36.2	0.20	0.96
Media	I	24.6	129.0	3.6	29.1	0.24	1.00
	II	30.1	95.7	4.0	28.8	0.21	1.00
	III	29.0	182.4	3.4	35.5	0.20	1.00
Adventitia	I	20.7	22.2	66.3	49.5	0.24	0.99
	II	26.5	13.7	40.9	48.8	0.17	0.99
	III	25.2	49.6	29.1	43.0	0.26	0.98

Parameters are defined in Eq. 8; R^2 , coefficient of determination of the simultaneous fitting of both circumferential and axial uniaxial tensile test data

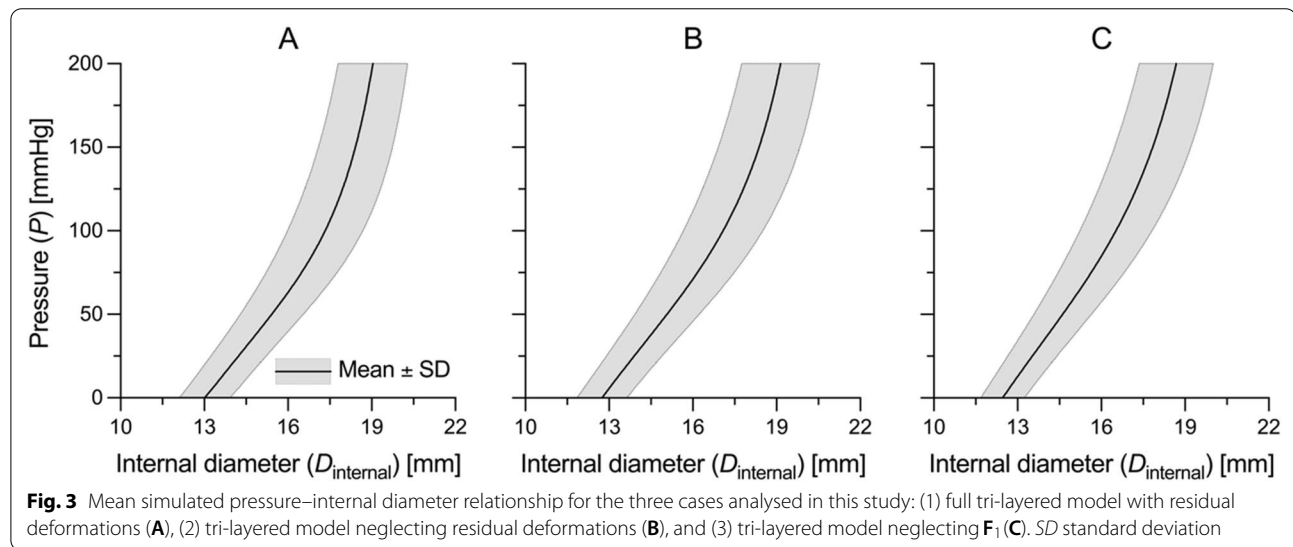
approximately twice as high in the adventitia ($135 \pm 25\%$ and $111 \pm 37\%$). As a result, while the intimal load bearing remained almost unaltered ($13 \pm 3\%$), medial and adventitial load bearings dropped and grew by $-6 \pm 3\%$ and $+7 \pm 4\%$, respectively. This shift in circumferential load bearing was caused by the biphasic $C_{\theta\theta\theta\theta}-P$

relationship of the adventitia; for pressures <90 mmHg, the adventitial $C_{\theta\theta\theta\theta}-P$ relationship was comparable to the intimal and medial relationships, which were nearly linear over the entire investigated pressure range (Fig. 4G). Conversely, adventitial stiffening with increasing pressure was markedly higher than that of both

Table 4 Layer-specific circumferential and axial components of the deformation gradients \mathbf{G}^k , \mathbf{F}_1 and $\mathbf{F}_{\text{residual},k} = \mathbf{F}_1 \mathbf{G}^k$.

\mathbf{G}^k	Intima		Media		Adventitia	
	$\hat{\lambda}_x^i$	$\hat{\lambda}_z^i$	$\hat{\lambda}_x^m$	$\hat{\lambda}_z^m$	$\hat{\lambda}_x^a$	$\hat{\lambda}_z^a$
I	1.04	1.02	1.04	0.99	0.94	1.02
II	1.02	1.05	1.03	0.97	0.98	0.99
III	1.03	1.00	1.01	0.99	0.97	1.02
Mean \pm SD	1.03 \pm 0.01	1.03 \pm 0.02	1.03 \pm 0.01	0.98 \pm 0.01	0.96 \pm 0.01	1.01 \pm 0.01
\mathbf{F}_1	Λ_Θ^i	Λ_Z^i	Λ_Θ^m	Λ_Z^m	Λ_Θ^a	Λ_Z^a
I	0.89	1.00	0.98	1.00	1.09	1.00
II	0.92	1.00	0.98	1.00	1.07	1.00
III	0.92	1.00	0.98	1.00	1.07	1.00
Mean \pm SD	0.91 \pm 0.01	1.00 \pm 0.00	0.98 \pm 0.00	1.00 \pm 0.00	1.07 \pm 0.01	1.00 \pm 0.00
$\mathbf{F}_{\text{residual},k} = \mathbf{F}_1 \mathbf{G}^k$	$\hat{\lambda}_x^i \Lambda_\Theta^i$	$\hat{\lambda}_z^i \Lambda_Z^i$	$\hat{\lambda}_x^m \Lambda_\Theta^m$	$\hat{\lambda}_z^m \Lambda_Z^m$	$\hat{\lambda}_x^a \Lambda_\Theta^a$	$\hat{\lambda}_z^a \Lambda_Z^a$
I	0.92	1.02	1.02	0.99	1.03	1.02
II	0.93	1.06	1.01	0.98	1.04	1.00
III	0.95	1.00	1.00	0.99	1.03	1.02
Mean \pm SD	0.93 \pm 0.01	1.03 \pm 0.02	1.01 \pm 0.01	0.98 \pm 0.00	1.04 \pm 0.00	1.01 \pm 0.01

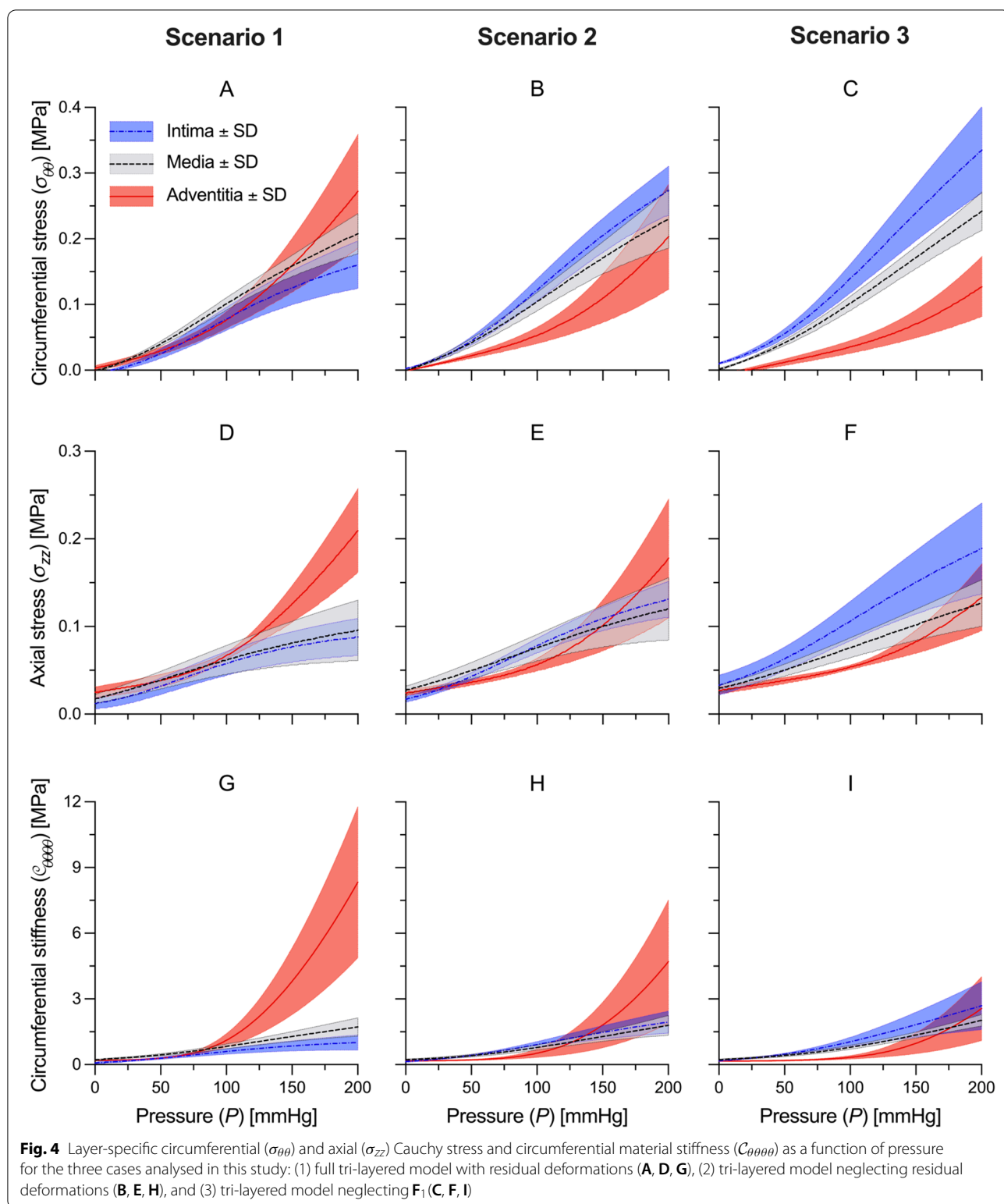
$\mathbf{F}_{\text{residual},k}$ defines the residual stretches experienced by each layer in the unload cylindrical vessel configuration (κ_{unloaded})



intima and media at pressures >90 mmHg, so that $C_{\theta\theta\theta\theta}$ at 160 mmHg was 4.20 ± 1.71 MPa for the adventitia, approximately three and four times higher than that of media (1.34 ± 0.28 MPa) and intima (0.95 ± 0.27 MPa), respectively.

Second, fully neglecting the layer residual stresses ($\mathbf{F}_{\text{residual},k} = \mathbf{I}$), strongly affected the distribution of both $\sigma_{\theta\theta}$ and σ_{zz} among layers; $\sigma_{\theta\theta}$ and σ_{zz} were highest and lowest at the intima and adventitia, respectively, over most of the investigated pressure range (Fig. 4B, E). At 100 mmHg, intimal $\sigma_{\theta\theta}$ and σ_{zz} and medial σ_{zz}

were $60 \pm 22\%$ ($p = 0.014$), $39 \pm 18\%$ ($p = 0.032$) and $24 \pm 9\%$ ($p = 0.018$) higher than corresponding values in the full model with residual stresses, respectively, while those of the adventitia were $32 \pm 5\%$ ($p = 0.091$) and $16 \pm 8\%$ ($p = 0.11$) lower. As a result, the intimal load bearing at 100 mmHg increased to $23 \pm 1\%$ ($p = 0.009$), that of the adventitia dropped to $16 \pm 2\%$ ($p = 0.002$), while that of the media was unaltered (Fig. 5C, D). Further, the shift in load bearing in response to the 60 mmHg pressure increase was milder at $-3 \pm 3\%$ and $+4 \pm 4\%$ for media and adventitia, respectively. Indeed, while



still exhibiting a biphasic $C_{\theta\theta\theta\theta}-P$ relationship, adventitial stiffening with increasing pressure was less marked than that observed for the model with residual stresses.

$C_{\theta\theta\theta\theta}$ at 160 mmHg was comparable in the three layers: 1.58 ± 0.34 MPa, 1.39 ± 0.26 MPa and 2.29 ± 1.35 MPa for intima, media and adventitia, respectively (Fig. 4H).

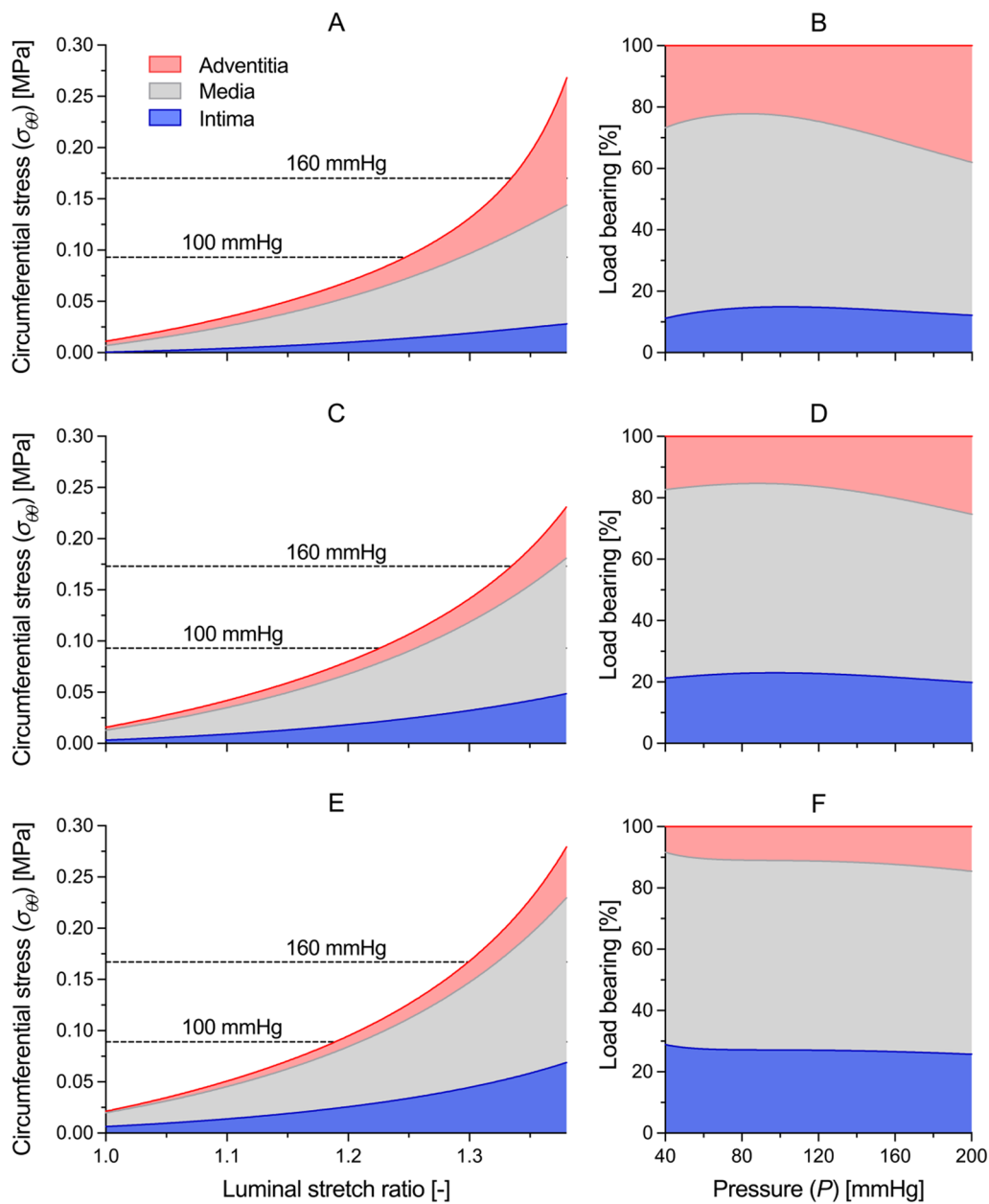


Fig. 5 Mean circumferential Cauchy stress–circumferential stretch relationships with load partitioning between layers and layer-specific circumferential load bearing for the three cases analysed in this study: (1) full tri-layered model with residual stresses (**A** and **B**), (2) tri-layered model neglecting residual stresses (**C** and **D**), and (3) tri-layered model neglecting F_1 (**E** and **F**). Circumferential stretch at the inner radius was computed as $\lambda_{\theta} = r_{\text{interna}}/R_{\text{interna}}$. In Panels A, C and E, the intimal line was obtained using Eq. 11 with $\sigma^m = \mathbf{0}$ and $\sigma^a = \mathbf{0}$, and the media line with $\sigma^a = \mathbf{0}$. The adventitial line was obtained using the full version of Eq. 14. This means that, for any given λ_{θ} /pressure, the amplitude of each coloured area is given by the corresponding layer’s circumferential stress multiplied by its loaded relative thickness (i.e. $\sigma_{\theta\theta}^k \frac{h^k}{h^{\text{wall}}}$ where k indicates a generic layer)

Third, Fig. 4C, F present the layer-specific $\sigma_{\theta\theta}$ and σ_{zz} as a function of pressure for the model where $F_{\text{residual},k} = G^k$ (i.e. neglecting the contribution of F_1). $\sigma_{\theta\theta}$ and σ_{zz} were lowest and highest at the adventitia and intima, respectively, throughout the entire investigated pressure range. Intimal $\sigma_{\theta\theta}$ and σ_{zz} at 100 mmHg

increased further to 0.140 ± 0.022 MPa (+ 82 ± 21% with respect to the full model, $p=0.010$, and + 14 ± 2% with respect to the model with no residual stresses, $p=0.041$) and 0.106 ± 0.022 MPa (+ 86 ± 14%, $p=0.028$, and + 35 ± 16%, $p=0.13$). Intimal circumferential load bearing at 100 mmHg increased to $27 \pm 2\%$ ($p=0.002$ and $p=0.013$

with respect to cases 1 and 2, respectively; Fig. 5E, F). Further, $C_{\theta\theta\theta}$ was lower in the adventitia than in the intima and media at most pressures (Fig. 4I), so that the adventitia did not act as a protective sleeve against high pressures. The shift in load bearing between adventitia and media when moving from 100 to 160 mmHg was negligible ($-1 \pm 2\%$ and $+2 \pm 2\%$, respectively).

4 Discussion

Residual stresses play a fundamental role in arterial mechanics [21, 22]. However, modelling residual stresses from complex three-dimensional geometrical features of layer-specific stress-free configurations is non-trivial [20, 27] and such stresses are hence sometimes neglected in experimental studies on arterial structure and mechanics [28, 29]. Using a recently developed tri-layered modelling framework that relies solely on data from wall and layer-specific uniaxial mechanical testing, this study aimed to illustrate the effects of totally or partially neglecting residual stresses on the mechanical behaviour of the tri-layered arterial wall [30].

In 1986, Chuong and Fung [21] were the first to estimate the distribution of stretches throughout the wall thickness of the unloaded rabbit thoracic aorta from measures of its OA. They found that the circumferential stretch ranged from approximately -0.86 at the luminal surface to 1.14 at the outer adventitial surface, crossing 1 (i.e. null deformation) at 37% of the wall thickness. More recently, Holzapfel and colleagues [20] developed a thick-walled modelling framework to estimate the three-dimensional layer-specific deformation of an unloaded vessel from measurements of the curvature of both circumferentially (i.e. estimating the OA) and axially oriented strips. When applied to the human aorta, their method estimated compression in both circumferential and axial directions for the intima, circumferential tension and axial compression for the media, and tension in both directions for the adventitia [20, 36]. In the present study, the circumferential stretch in κ_{unloaded} was 0.93 for the intima, 1.01 for the media and 1.04 for the adventitia. It is worth noting, however, that, given the thin-walled modelling approach used here, these values refer to the mid-wall point of each layer and are assumed to be constant throughout the layer thickness. The intimal, medial and adventitial mid-wall points were located at approximately 9%, 42% and 85% of the total wall thickness from the luminal surface, respectively. Therefore, deformations at the luminal and outer adventitial surface likely exceed average values for the intima and adventitia [21].

The inflation of a cylindrical structure induces circumferential deformations that decrease monotonically from the luminal surface to the outer surface of the adventitia (see Eq. 6). Researchers generally agree that residual

stresses aim at counterbalancing this effect, guaranteeing an almost uniform distribution of stresses throughout the wall thickness in the physiological range of pressures [21, 24, 36]. Indeed, when residual stresses were included in the tri-layered arterial model, the stress-pressure relationships of intima, media, and adventitia were almost superimposed throughout most of the pressure range investigated in this study. However, at high pressures (i.e. >140–150 mmHg), the adventitial stress considerably deviated from that of the intima and media due to its rapid stiffening with increasing pressure. This finding suggests a strong functional coupling between the layer-specific microstructure, mechanical properties, and deposition stretches (i.e. $F_{\text{residual},k}$), allowing the adventitia to behave similarly to intima and media at normal physiological pressures and act as a protective sleeve that preserves the wall integrity at high- and supra-physiological pressures [2].

In agreement with previous findings [37], neglecting the layer-specific residual stresses affected the role individual layers play in the macroscopic behaviour of the wall; the intimal load bearing increased from 16 to 23%, reflecting a 55% increase in its circumferential stress. Furthermore, the adventitia lost its role of protective layer at high pressures. Recently, De Lucio et al. [28] performed a finite element simulation of the inflation of a tri-layered model of the human aneurysmatic aorta using previously determined layer-specific HGO-SEF model parameters of the human abdominal aorta with non-atherosclerotic intimal thickening [13]. Their model did not account for residual stresses (comparable to scenario 2 in our study) and estimated that the intima, constituting approximately 25% of the wall thickness, bore approximately 71% of the circumferential load, with only marginal contributions from media (14%) and adventitia (15%). While the non-atherosclerotic intimal thickening and the pathological geometrical features of the aneurysmatic wall likely contributed to concentrating circumferential stresses at the intima, these findings need to be considered with caution since neglecting the layer-specific residual stresses of the aneurysmatic wall [18] likely considerably altered the distribution of stresses across the wall thickness.

Among experimental methods, tension–inflation experiments most closely mimic the physiological multi-directional loading condition the arterial wall is subjected to in vivo [38]. However, the required specialised equipment is not available in every biomechanics laboratory and might pose some limits when simultaneously imaging the wall microstructure in human-sized arteries [6]. Therefore, planar uniaxial and biaxial tensile tests are still widely used to investigate arterial mechanics and microstructure ex vivo [10–14, 17]. Their inherent methodological limitations should, however, always be considered

when analysing their results, and the tri-layered modelling framework herein represents an attempt, in part, to address this issue. For example, planar uniaxial and biaxial tensile tests are commonly used to estimate functions that define the collagen recruitment with increasing stretch [39, 40]. Chow and colleagues [11] combined planar biaxial mechanical testing (comparable to scenario 3 in our study) and multiphoton microscopy to investigate the rearrangement of collagen and elastin microstructures in response to load and found that the recruitment of adventitial collagen showed a 20% strain delay with respect to that of the media. It is worth noting, however, that our model predicted a 7% circumferential elongation of the adventitia in the deformation from $\kappa_{\text{composite}}$ to κ_{unloaded} (\mathbf{F}_1). This deformation would compensate, at least in part, the observed delayed recruitment of adventitial collagen. Indeed, in our model, neglecting \mathbf{F}_1 considerably limited the contribution of the adventitia to the macroscopic wall behaviour (Fig. 4C, F, I).

4.1 Limitations

In this study, the three layers were modelled as three concentric membranes (thin-walled approach). Therefore, all modelled parameters, including $\mathbf{F}_{\text{residual},k}$, and biomechanical variables represent mean values across the layer thickness. In reality, arterial layers are not as homogeneous and $\mathbf{F}_{\text{residual},k}$ is not constant across the layer thickness. This leads to the existence of layer-specific opening angles, possibly affecting the stress distribution across the layer thickness [14, 20]. A thick-walled modelling approach would further refine the analysis, but model complexity would also increase considerably as would the complexity of estimating the related geometrical parameters (layers' three-dimensional curvatures).

The layer-specific model parameters were estimated by fitting the intact wall and layer-specific response to uniaxial testing in the circumferential and axial directions, simultaneously, as done previously [13, 14, 30]. While this approach indirectly yields biaxial information, biaxial experiments could further refine our analysis, providing direct information on the coupling between circumferential and axial responses.

We did not perform any imaging of the layers' cross-section to visually verify the accuracy of the peeling process. Nevertheless, layer-specific thicknesses found here are in line with those reported in other studies [13, 14, 41]. Further, the thickness of each layer was measured three times along the strip length, thus allowing to evaluate whether the peeling process was performed uniformly. Layer-specific inter-sample standard deviations of the thickness were comparable to those found in the

intact wall (on average 5–9% of the sample thickness). This suggests that the variability in layer thickness along the sample length mainly reflected actual variability in intact wall thickness [42] rather than being a sign of sub-optimal layer separation.

5 Conclusions

In this study, a recently developed tri-layered modelling framework was used to investigate the effect of residual stresses on the mechanics of the tri-layered arterial wall. While isolated layers exhibited considerably different behaviour, their pre-deformed state make their response strikingly similar at physiological pressures. Conversely, at high pressures, the adventitial mechanical response deviated from that of intima and media, conferring its protective function.

Abbreviations

a: Adventitia; α : Collagen fibre orientation parameter; \mathbf{c}_1 : Collagen fibre stiffness-like parameter; \mathbf{c}_2 : Collagen fibre non-linearity parameter; \mathbf{C} : Right Cauchy–Green strain tensor; \mathbf{C} : Wall material stiffness; \mathbf{F}_1 : Deformation gradient mapping the deformation from $\kappa_{\text{composite}}$ to κ_{unloaded} ; \mathbf{F}_2 : Deformation gradient mapping the deformation from κ_{unloaded} to $\kappa_{\text{tension-inflation}}$; \mathbf{G}^k : Layer-specific deformation gradient mapping the deformation from κ_{isolated} to $\kappa_{\text{composite}}$; HGO: Holzapfel–Gasser–Ogden; h : Arterial wall thickness in $\kappa_{\text{tension-inflation}}$; i: Intima; κ_{isolated} : Isolated layer configuration in Cartesian coordinates $(\mathcal{X}, \mathcal{Y}, \mathcal{Z})$; $\kappa_{\text{composite}}$: Flat, tri-layered wall configuration in Cartesian coordinates $(\mathcal{X}, \mathcal{Y}, \mathcal{Z})$; κ_{unloaded} : Unloaded, cylindrical, tri-layered vessel configuration in cylindrical coordinates (Θ, R, Z) ; $\kappa_{\text{tension-inflation}}$: Axially stretch and pressurised, cylindrical, tri-layered vessel configuration in cylindrical coordinates (θ, r, z) ; l_j : Length of the flat, tri-layered wall in the j -direction; L_j^k : Length of the isolated layer k in the j -direction; $\hat{\lambda}_j^k$: j -direction component of \mathbf{G}^k ; Δ_j : j -direction component of \mathbf{F}_1 ; λ_j : j -direction component of \mathbf{F}_2 ; m: Media; μ : Elastin stiffness-like parameter; OA: Opening angle; Ψ : Strain energy function; R_{internal} : Unloaded luminal radius; r_{internal} : Loaded luminal radius; ρ : Collagen fibre dispersion parameter; SEF: Strain energy function; $\boldsymbol{\sigma}$: Modelled Cauchy stress tensor; $\boldsymbol{\sigma}_{\text{exp}}$: Modelled Cauchy stress tensor.

Acknowledgements

We thank Ashraf W. Khir for his support and valuable advice.

Author Contributions

AG and BS contributed to the study conception and to the development of the tri-layered modelling framework used in the study. AG contributed to the experimental data collection and analysis, and to the manuscript drafting. BS contributed to the critical appraisal and manuscript editing.

Funding

This work was supported by the ARTERY (Association for Research into Arterial Structure and Physiology) society (2019 Research Exchange Grant to AG) and by the European Union's Horizon 2020 Research and Innovation programme (Grant 793805 to BS). The sole role of the funding sources was providing financial contribution.

Availability of Data and Materials

The data supporting this study are available from the corresponding author.

Declarations

Conflict of Interest

The authors declare that they have no competing interest.

Ethics Approval

N/A.

Consent to Participate

N/A.

Consent for Publication

The authors give their consent for publication of this manuscript.

Author details

¹Biomedical Engineering Theme, Brunel University London, Kingston Lane, Uxbridge UB8 3PH, UK. ²Department of Biomedical Engineering, School of Engineering and Applied Science, Yale University, 55 Prospect St, New Haven, CT 06511, USA. ³Department of Biomedical Engineering, CARIM School for Cardiovascular Diseases, Maastricht University, Universiteitssingel 50, Room 3.353, 6229 ER Maastricht, The Netherlands. ⁴GROW School for Oncology and Developmental Biology, Maastricht University, Universiteitssingel 40, 6229 ER Maastricht, The Netherlands.

Received: 17 November 2021 Accepted: 23 February 2022

Published online: 4 April 2022

References

- Wolinsky H, Glagov S. A lamellar unit of aortic medial structure and function in mammals. *Circ Res*. 1967;20:99–111.
- Burton AC. Relation of structure to function of the tissues of the wall of blood vessels. *Physiol Rev*. 1954;34:619–42.
- Wolinsky H, Glagov S. Structural basis for the static mechanical properties of the aortic media. *Circ Res*. 1964;14:400–13.
- O’Connell MK, Murthy S, Phan S, Xu C, Buchanan J, Spilker R, et al. The three-dimensional micro- and nanostructure of the aortic medial lamellar unit measured using 3D confocal and electron microscopy imaging. *Matrix Biol*. 2008;27:171–81.
- Schriefl AJ, Wolinski H, Regitnig P, Kohlwein SD, Holzapfel GA. An automated approach for three-dimensional quantification of fibrillar structures in optically cleared soft biological tissues. *J R Soc Interface*. 2013;10:20120760.
- Giudici A, Wilkinson IB, Khir A. Review of the techniques used for investigating the role of elastin and collagen in arterial wall mechanics. *IEEE Rev Biomed Eng*. 2021;14:256–69.
- Akhtar R, Sherratt MJ, Watson REB, Kundu T, Derby B. Mapping the micro-mechanical properties of cryo-sectioned aortic tissue with scanning acoustic microscopy. *Mater Res Soc Symp Proc*. 2009;1132:1132-Z03-07.
- Rezakhaniha R, Agianniotis A, Schrauwen JTCJ, Griffa A, Sage D, Bouten CVCC, et al. Experimental investigation of collagen waviness and orientation in the arterial adventitia using confocal laser scanning microscopy. *Biomech Model Mechanobiol*. 2012;11:461–73.
- Berry CL, Greenwald SE, Rivett JF. Static mechanical properties of the developing and mature rat aorta. *Cardiovasc Res*. 1975;9:669–78.
- Gundiah N, Babu AR, Pruitt LA. Effects of elastase and collagenase on the nonlinearity and anisotropy of porcine aorta. *Physiol Meas*. 2013;34:1657–73.
- Chow M-J, Turcotte R, Lin CP, Zhang Y. Arterial extracellular matrix: a mechanobiological study of the contributions and interactions of elastin and collagen. *Biophys J*. 2014;106:2684–92.
- Krasny W, Morin C, Magoaric H, Avril S. A comprehensive study of layer-specific morphological changes in the microstructure of carotid arteries under uniaxial load. *Acta Biomater*. 2017;57:342–51.
- Weisbecker H, Pierce DM, Regitnig P, Holzapfel GA. Layer-specific damage experiments and modeling of human thoracic and abdominal aortas with non-atherosclerotic intimal thickening. *J Mech Behav Biomed Mater*. 2012;12:93–106.
- Peña JA, Martínez MA, Peña E. Layer-specific residual deformations and uniaxial and biaxial mechanical properties of thoracic porcine aorta. *J Mech Behav Biomed Mater*. 2015;50:55–69.
- Holzapfel GA, Gasser CT, Sommer G, Regitnig P. Determination of layer-specific mechanical properties of human coronary arteries with nonatherosclerotic intimal thickening and related constitutive modeling. *Am J Physiol*. 2005;289:H2048–58.
- Schulze-Bauer CAJ, Regitnig P, Holzapfel GA. Mechanics of the human femoral adventitia including the high-pressure response. *Am J Physiol Hear Circ Physiol*. 2002;282:2427–40.
- Sommer G, Holzapfel GA. 3D constitutive modeling of the biaxial mechanical response of intact and layer-dissected human carotid arteries. *J Mech Behav Biomed Mater*. 2012;5:116–28.
- Devege RP, Iliopoulos DC, Kritharis EP, Angouras DC, Sfyris D, Papadodima SA, et al. Effect of aneurysm and bicuspid aortic valve on layer-specific ascending aorta mechanics. *Ann Thorac Surg*. 2018;106:1692–701.
- Sassani SG, Tsangaris S, Sokolis DP. Layer- and region-specific material characterization of ascending thoracic aortic aneurysms by microstructure-based models. *J Biomech*. 2015;48:3757–65.
- Holzapfel GA, Ogden RW. Modelling the layer-specific three-dimensional residual stresses in arteries, with an application to the human aorta. *J R Soc Interface*. 2010;7:787–99.
- Chuong CJ, Fung YC. On residual stresses in arteries. *J Biomech Eng*. 1986;108:189–92.
- Rachev A, Greenwald SE. Residual strains in conduit arteries. *J Biomech*. 2003;36:661–70.
- Alastrué V, Peña E, Martínez MA, Doblaré M. Assessing the use of the “opening angle method” to enforce residual stresses in patient-specific arteries. *Ann Biomed Eng*. 2007;35:1821–37.
- Humphrey J, Na S. Elastodynamics and arterial wall stress. *Ann Biomed Eng*. 2002;30:509–23.
- Vaishnav RN, Vassoughi J. Residual stress and strains in aortic segments. *J Biomech*. 1987;20(3):235–9.
- Greenwald SE, Moore JJE, Rachev A, Kane TPC, Meister J-J. Experimental investigation of the distribution of the residual strains in the arterial wall. *Trans ASME*. 1997;119:438–44.
- Pierce DM, Fastl TE, Rodríguez-Vila B, Verbrugge P, Fournneau I, Maleux G, et al. A method for incorporating three-dimensional residual stretches/stresses into patient-specific finite element simulations of arteries. *J Mech Behav Biomed Mater*. 2015;47:147–64.
- de Lucio M, García MF, García JD, Rodríguez LER, Marcos FÁ. On the importance of tunica intima in the aging aorta: a three-layered in silico model for computing wall stresses in abdominal aortic aneurysms. *Comput Methods Biomech Biomed Eng*. 2020;22:1–18.
- Zahedmanesh H, John KD, Lally C. Simulation of a balloon expandable stent in a realistic coronary artery—determination of the optimum modelling strategy. *J Biomech*. 2010;43:2126–32.
- Giudici A, Khir AW, Szafron JM, Spronck B. From uniaxial testing of isolated layers to a tri-layered arterial wall: a novel constitutive modelling framework. *Ann Biomed Eng*. 2021;49:2454–67.
- Carew TEE, Vaishnav RN, Patel DJ. Compressibility of the arterial wall. *Circ Res*. 1968;XXIII:61–8.
- Gasser TC, Ogden RW, Holzapfel GA. Hyperelastic modelling of arterial layers with distributed collagen fibre orientations. *J R Soc Interface*. 2006;3:15–35.
- Duprey A, Khanafer K, Schlicht M, Avril S, Williams D, Berguer R. In vitro characterisation of physiological and maximum elastic modulus of ascending thoracic aortic aneurysms using uniaxial tensile testing. *Eur J Vasc Endovasc Surg*. 2010;39:700–7.
- Van Loon P, Klip W, Bradley EL. Length-force and volume-pressure relationships of arteries. *Biorheology*. 1977;14:181–201.
- Baek S, Gleason RL, Rajagopal KR, Humphrey JD. Theory of small on large: potential utility in computations of fluid–solid interactions in arteries. *Comput Methods Appl Mech Eng*. 2007;196:3070–8.
- Zheng X, Ren J. Effects of the three-dimensional residual stresses on the mechanical properties of arterial walls. *J Theor Biol*. 2016;393:118–26.
- Díaz C, Peña JA, Martínez MA, Peña E. Unraveling the multilayer mechanical response of aorta using layer-specific residual stresses and experimental properties. *J Mech Behav Biomed Mater*. 2021;113:104070.
- van der Bruggen MM, Reesink KD, Spronck PJM, Bitsch N, Hameleers J, Megens RTA, et al. An integrated set-up for ex vivo characterisation of biaxial murine artery biomechanics under pulsatile conditions. *Sci Rep*. 2021;11:2671.
- Wang Y, Zeinali-Davarani S, Zhang Y. Arterial mechanics considering the structural and mechanical contributions of ECM constituents. *J Biomech*. 2016;49:2358–65.

40. Polzer S, Gasser TC, Novak K, Man V, Tichy M, Skacel P, et al. Structure-based constitutive model can accurately predict planar biaxial properties of aortic wall tissue. *Acta Biomater.* 2015;14:133–45.
41. Sokolis DP. Regional distribution of layer-specific circumferential residual deformations and opening angles in the porcine aorta. *J Biomech.* 2019;96:109335.
42. Kim J, Baek S. Circumferential variations of mechanical behavior of the porcine thoracic aorta during the inflation test. *J Biomech.* 2011;44:1941–7.

Ready to submit your research? Choose BMC and benefit from:

- fast, convenient online submission
- thorough peer review by experienced researchers in your field
- rapid publication on acceptance
- support for research data, including large and complex data types
- gold Open Access which fosters wider collaboration and increased citations
- maximum visibility for your research: over 100M website views per year

At BMC, research is always in progress.

Learn more biomedcentral.com/submissions

